Comparing Undecimated Wavelet, Nonsubsampled Contourlet and Shearlet Transform for SAR Image Despeckling

Saeed Jafari, Sedigheh Ghofrani, and M. Sheikhan
Electrical and Electronic Engineering Department, Islamic Azad University, Tehran South Branch
Tehran, Iran
E-mail: st_saeed_jafari@azad.ac.ir, s_ghofrani@azad.ac.ir(Corresponding author), msheikhn@azad.ac.ir

Received: October 2014 Revised: Dec. 2014 Accepted: Feb. 2015

ABSTRACT:
Synthetic Aperture Radar (SAR) images suffer of multiplicative speckle noise, which damages the radiometric resolution of SAR images and makes the data interpretation difficult. Bayesian shrinkage in a transformed domain is a well-known method based on finding threshold value to suppress the speckle noise. This paper present a new approach to obtain the optimum threshold values for Bayesian shrinkage. For this purpose, we use undecimated wavelet transform (UWT), nonsubsampled Contourlet transform (NSCT), and nonsubsampled Shearlet transform (NSST). According to our experimental results, transformed coefficients influenced by noise differently. It means that some coefficients in transformed domain belong to the specific subband are more robust against noise. We use this new found property in order to determine the optimum threshold value and developed our proposed method named weighted Bayesian Shrinkage in transformed domain. Our experimental results show that finding the optimum threshold value in Shearlet domain outperforms both Contourlet and undecimated wavelet transform. Although the weighted Bayesian Shrinkage in NSCT used before, the weighted Bayesian Shrinkage in NSST is applied in this paper for the first time.

KEYWORDS: Undecimated wavelet transform, Nnonsubsampled Contourlet transform, Nonsubsampled Shearlet transform, SAR images despeckling, Weighted Bayesian Shrinkage

.

1. INTRODUCTION

SAR provides the capability for all-weather and day-or-night operation. There are wide variety of applications for SAR images such as reconnaissance, surveillance, automatic target recognition, deforestation, ice flows, and oil spills. However, for any coherent imaging like SAR and ultrasound, the multiplicative speckle noise damages the radiometric resolution. Therefore, it is necessary to suppress the speckle noise before processing like image segmentation, edge detection, and object tracking. In general, SAR despeckling approaches grouped into two main classes; spatial filtering methods and transformed domain methods. The main challenges for any despeckling methods are reducing the speckle noise and preserving edges and textures. SAR image denoising in spatial domain including Lee filter [1], Frost filter [2], Kuan filter [3] and total variation [4], needs low computational complexity but fails to preserve effectively the details. Among many transformed domain methods, we refer to adaptive wavelet thresholding [5], Bayesian denoising in wavelet domain [6], Gauss–Markov random fields in wavelet domain [7], hidden Markov tree and Gauss-Markov models in Contourlet domain [8] and SAR images despeckling based on NSST [9]. Since two-dimensional separable wavelet transform (WT) constructed from tensor products of one-dimensional wavelets, images with discontinuities and singularities, cannot be optimal represented by two-dimensional WT. Furthermore, the traditional wavelet has a limited capability in handling directional information. To dominate limitation, many methods have proposed in recent years. These methods include Curvelet [10], Contourlet [11], Shearlet [12], Complex wavelet [13] and Ridgelet [14].The well-known transform was proposed by Do and Vetterli [11] offers a flexible multi-resolution, local and directional image representation by using contour segments, so it named Contourlet transform (CT). Its base function with two additional properties viz directionality and anisotropy can effectively capture the geometric regularity in the image. It adaptively gives the optimal representation of an image.

Recently, Shearlet constructed based on affine system with synthetics and expansion, which can sparsely represent an image and give an optimal approximation of it. It also has flexible direction selectivity like Curvelet but easier to implement. The original WT, CT, and Shearlet transform (ST) were shift variant. That means, the coefficients are changing whenever the original signal is translating. In general, using up- and down-

sampling makes a transform being shift variant. Thereby, the pseudo-Gibbs phenomena seen around singularities for any shift variant transform. Anyway, omitting the up- and down-sampling blocks introduced UWT [15-16], NSCT [17], and NSST [18]. As the coefficients do not decimate between the decomposition levels, all subbands sizes are the same as the original input image. It was shown that the UWT outperforms the original WT for both additive and multiplicative noise reduction [19].

In order to have a comparison among UWT, NSCT, NSST coefficients and see the robustness Shearlet directionality, we have chosen Zoneplate as a test image and show the numbered subbands and the corresponding coefficients belong to two level decomposition in Figs. 1-3.

In this work, we apply our improved method in transformed domain based on thresholding technique. In general, Bayesian Shrinkage is working based on finding the threshold values. We use this method for three mentioned transforms coefficients, so named them as BS-UWT, BS-NSCT, and BS-NSST. In addition, we find noise efficiency coefficients for any subband in transformed domain and combine with Bayesian shrinkage to find the optimum threshold values. In general, the new method named weighted Bayesian (WBS) and for three referred transforms, we named them WBS-UWT, WBS-NSCT, WBS-NSST.

The paper is organized as follows: In Section 2, the speckle noise model and despeckling in transformed domain by thresholding are explained. Our proposed method for denoising in transformed domain based on considering the noise efficiency is expressed in Section 3. Section 4 shows our experimental results and has comparison among six methods for analyzing a synthetic image as well as a real SAR image. Finally, we have conclusion in Section 5.

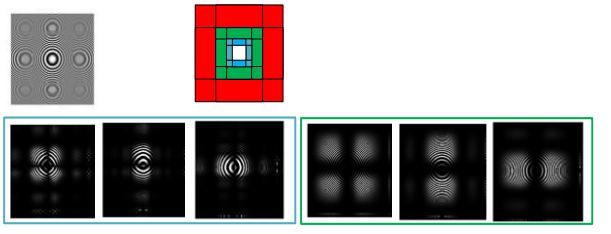

Fig. 1. Shown the original Zoneplate image, tiling of the frequency plane, decomposition coefficients belong to the second and third level of UWT.

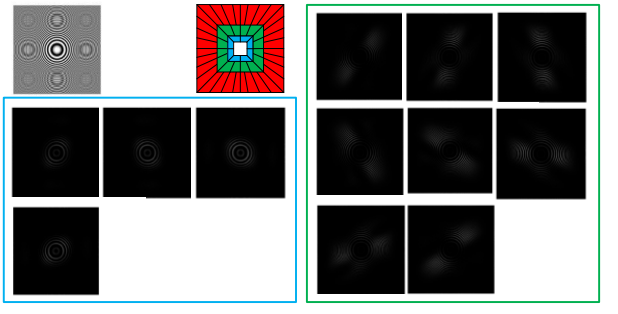

Fig. 2. Shown the original Zoneplate image, tiling of the frequency plane, decomposition coefficients belong to the second and third level of NSCT.

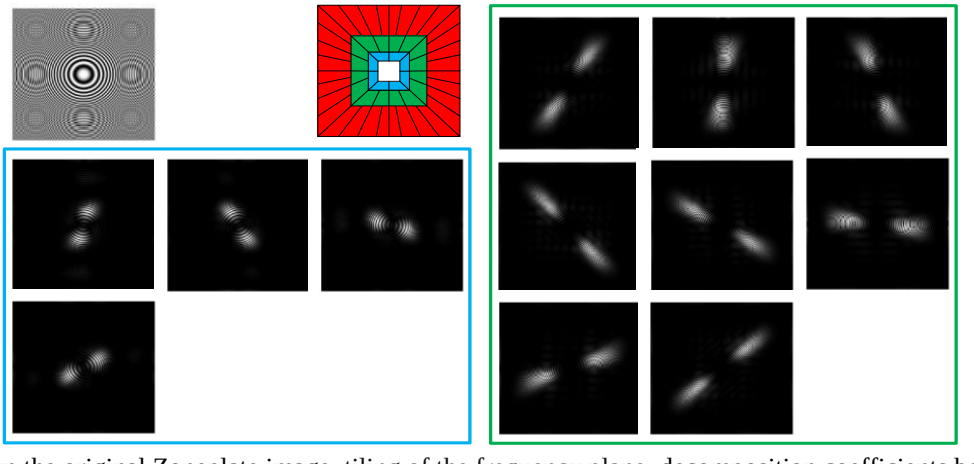

Fig. 3. Shown the original Zoneplate image, tiling of the frequency plane, decomposition coefficients belong to the second and third level of NSST.

2. BACKGROUND

2.1. Speckle Noise Model

As we know, the noise of SAR images named speckle is multiplicative. It must be stressed that speckle is noise like, but it is not noise; it is a real electromagnetic measurement, which is exploited, for example, in SAR interferometry [20]. Therefore, when the radar scans a uniform surface, the SAR images have emerged in dramatic changes in the gray, and some resolution cell is a dark spot, and some resolution cell is a bright spot,

showing a granular ups and downs. The spots rooted in a coherent superposition of radar echo are called speckle noise. Generally, the coherent speckle noise was developed in [21]. The multiplicative model is

$$G(x,y) = S(x,y) + S(x,y)\tilde{N}(x,y) \quad (1)$$

Where, (x,y) is the pixel position. G refers to the image corrupted by speckle noise. S denotes the noise free signal, and $\tilde{N}$ is speckle noise. Eq. (1) can be written as:

$$G(x,y) = S(x,y)N(x,y) \quad (2)$$

Where, $N(x,y) = 1 + \tilde{N}(x,y)$. In order to convert the multiplicative noise into additive noise, we use the homomorphic framework, which means using the logarithm transform before processing and the exponential transform at the end. By using the logarithm transform of Eq. (2), we have

$$g(x,y) = s(x,y) + n(x,y) \quad (3)$$

Where $s(x,y) = \log S(x,y)$ and $n(x,y) = \log N(x,y)$ are noise free signal and the additive noise, respectively. The noise is considered white Gaussian, zero mean, and independent of signal.

2.2. Denoising in Transformed Domain

The goal is to retrieve $\hat{S}(x,y)$ as an estimate of image $S(x,y)$ from noisy observation $G(x,y)$. Let $T(.)$ and $T^{-1}(.)$ denote the forward and inverse transform operators. An image denoising algorithm has the following steps.

- Perform decomposition using UWT, NSCT, and NSST (which are linear [22]-[23]-[24]) by applying $T(.)$ to Eq. (3).

$$D_g^{l,k} = T(g(x,y)) = T(s(x,y) + n(x,y)) = D_s^{l,k} + D_n^{l,k} \quad (4)$$

where *l*, *k* are the decomposition level and subband, $D_g^{l,k}$ refers the image corrupted by speckle noise, $D_s^{l,k}$ denotes the noise free signal, and $D_n^{l,k}$ is the additive noise in transformed domain.

- Calculate threshold value of detailed parts using shrinkage rules.
- Apply soft thresholding to the noisy coefficients.
- Use $T^{-1}(.)$ operator to reconstruct the denoised image.

Thresholding method is a simple non-linear technique that is sensitive to noise components. In this method, thresholding operates on coefficients in transformed domain, small coefficients are dominated by noise, and however coefficients with a large absolute value carry more signal information than noise. In its most basic form, noisy coefficients, with small values, set to zero and an inverse transform may result the less noisy signal.

It is important to know about three ways of thresholding on transformed domain coefficients. They are hard thresholding, soft thresholding and semi-soft thresholding.

In hard thresholding, as written in Eq. (5), all coefficients whose magnitude is smaller than the selected threshold value λ are set to zero and the others whose magnitude is greater than λ remains as they were.

$$D_{\hat{s}_i}^{l,k} = \begin{cases} D_{g_i}^{l,k} & ;|D_{g_i}^{l,k}| \geq \lambda \\ 0 & ;|D_{g_i}^{l,k}| < \lambda \end{cases} \quad (5)$$

In soft thresholding, as written in Eq. (6), the coefficients with greater magnitude than the threshold value λ are shrunk towards zero and other coefficients set to zero.

$$D_{\hat{s}_i}^{l,k} = \begin{cases} sign(D_{g_i}^{l,k})(|D_{g_i}^{l,k}| - \lambda) & ;|D_{g_i}^{l,k}| \geq \lambda \\ 0 & ;|D_{g_i}^{l,k}| < \lambda \end{cases} \quad (6)$$

The aim of semi-soft thresholding is to offer a compromise between hard and soft thresholding by changing the gradient of the slope. This scheme requires two thresholds, a lower threshold λ_1 and an upper threshold λ_2 where λ_2 is estimated to be twice the value of lower threshold λ_1.

$$D_{\hat{s}_i}^{l,k} = \begin{cases} 0 & ;|D_{g_i}^{l,k}| \leq \lambda_1 \\ sign(D_{g_i}^{l,k}) \dfrac{\lambda_2(|D_{g_i}^{l,k}| - \lambda_1)}{\lambda_2 - \lambda_1} & ;\lambda_1 < |D_{g_i}^{l,k}| \leq \lambda_2 \\ D_{g_i}^{l,k} & ;|D_{g_i}^{l,k}| > \lambda_2 \end{cases} \quad (7)$$

Where in Eqs. (5) - (7), $D_{g_i}^{l,k}$ and $D_{\hat{s}_i}^{l,k}$ are input and output coefficients, λ, λ_1 and λ_2 are the threshold limits. Some well-known thresholding methods are VisuShrink [25], SureShrink [26] and BayesShrink [5] methods. The main goal in thresholding method is finding the optimum threshold value. This threshold can be adaptive or nonadaptive per subband. VisuShrink is a non-adaptive universal threshold and SureShrink and BayesShrink are adaptive threshold methods.

VisuShrink was introduced by Donoho is the simplest way to find a threshold value for denoising. It uses a threshold value that is proportional to the standard deviation of the noise [27]-[28]. The inheritage of finding the threshold value by this method is discarding many coefficients and therefore result a blurred image. In order to overcome this problem, the threshold value was obtained based on Stein's unbiased risk estimator which named SureShrink [26]. In this method, the threshold value for every decomposition level is obtained adaptively. While SureShrink obtains a

threshold value for each decomposition level including different subbands, the BayesShrink [5] computes the optimum threshold values at

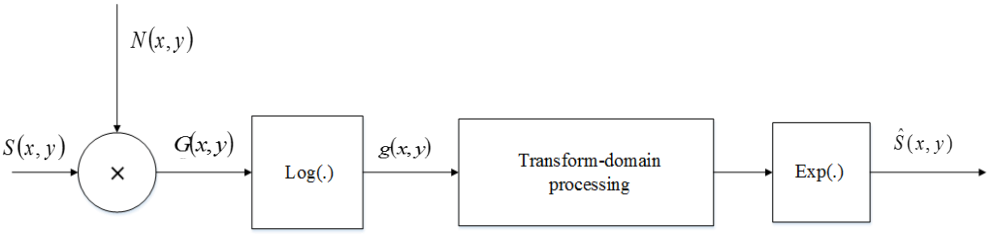

Fig. 4. The block diagram of speckle denoising in transformed domain

each decomposition level and for every subbands separately, according to

$$t_B = \frac{\sigma^2_{D_n^{l,k}}}{\sigma_{D_s^{l,k}}} \quad (8)$$

Where t_B is BayesShrink threshold, $\sigma^2_{D_n^{l,k}}$ is noise variance and $\sigma_{D_s^{l,k}}$ is noise free signal power in transformed domain for decomposition level l and subband k. As we use the BayesShrink for three transformed domain, we named them BS-UWT, BS-NSCT, and BS-NSST.

3. OUR PROPOSED METHOD

The general block diagram of our proposed method is shown in Fig. 4, where the center block is thresholding operator in transformed domain. BayesShrink is a popular thresholding method that can be applied in Shearlet, Contourlet [29] and wavelet transform domain [30]. Finding the optimum threshold value to get an output image with the least blurring effect and the most noise reduction is the main goal of any algorithm. In order to implement the BayesShrink in transformed domain based on Eq. (8), the noise variance and the free noise signal variance are to estimate for each subband. The standard deviation of noise $\sigma_{D_n^{l,k}}$ in BayesShrink method is estimated by

$$\sigma_{D_n^{l,k}} = \frac{\text{median}(D_g^{l,k})}{0.6745} \quad (9)$$

Where $D_g^{l,k}$ refers to the coefficients of l-th level and k-th subband in transformed domain. Since the additive noise and the signal are supposed to be independent, according to Eq. (3), we assume that the signal coefficients and noise coefficients are also independent in transformed domain, i.e. $\sigma^2_{D_g^{l,k}} = \sigma^2_{D_s^{l,k}} + \sigma^2_{D_n^{l,k}}$ where $\sigma^2_{D_s^{l,k}}$ is the signal variance without noise, and $\sigma^2_{D_g^{l,k}}$ is the variance of noisy signal for decomposition level l and subband k. It was shown [29] that the variance of free noise signal can be estimated as, $\sigma^2_{D_s^{l,k}} = \max(\sigma^2_{D_g^{l,k}} - \sigma^2_{D_n^{l,k}}, 0)$. We use local variance estimation method for estimating the variance of noisy signal [31]. In BayesShrink method, the noise variance approximated by robust median estimator Eq. (9), and the signal variance without noise estimated for any subbands individually. Then, the optimum threshold value for any subbans, t_B, is obtained using Eq. (8).

In [32], it was shown that the Contourlet coefficients belong to the specific subbands are more robust against noise. They [32] used this property in order to determine the optimum threshold value and named as weighted Bayesian shrinkage. In this paper, we show that this property is also satisfied for NSCT and NSST as well. So, the weighted threshold for each subband is

$$t_{wB} = \alpha t_B \quad (10)$$

Where α is the weighting factor that may vary for different subbands and t_{wB} is the new soft threshold value. Our experimental results show that, in presence of multiplicative speckle noise or additive Gaussian noise regardless of image type and noise power, the transform coefficients belong to different subbands may not have the same behavior. It means some coefficient belong to specific subbands are more robust against noise. In order to show this property, we consider Barbara with size 512×512 pixels as a test image. The original noise free test image and the noisy image decomposed to three levels by UWT, NSCT and NSST. The Mean Square Error (MSE) of noise free and noisy image transform coefficients are obtained for each decomposition level l , and, subband k,

$$MSE_{l,k} = \frac{1}{mn}\sum_{i=1}^{m}\sum_{j=1}^{n}(D_g^{l,k}(i,j) - D_s^{l,k}(i,j))^2 \quad (11)$$

Where $D_g^{l,k}$ and $D_s^{l,k}$ denote the transformed coefficients of signal that is corrupted by speckle noise and the original noise free, and mn is the transform coefficients size. Obviously, the size of the original image is the same as all coefficients at each level and subband for UWT, NSCT, and NSST as well. We were

interested in performing experiments on images of different types and with various contents in order to be able to obtain results, which we could claim to be general enough. The MSEs of ten independent trials for the NSST, NSCT, and UWT coefficients on four different images are shown in Fig. 5. As seen in Fig. 5, for NSCT and NSST, some subbands are more robust against noise in comparison with beside subbands.

In real application, including SAR images, there is not a clean signal or noise free signal. So, a white image as a flat image whose pixels have the same gray scale considered as the noiseless signal.

Now we can determine the weighting factor, α, for each decomposition level, *l*, and subband, *k*, and find the optimum threshold value based on Eq. (10), for speckle denoising. The weighting factor is,

$$\alpha_{l,k} = \frac{MSE_{l,k}}{\overline{MSE}_l} \tag{12}$$

Where $\overline{MSE}_l$ is the average MSEs of subbands,

$$\overline{MSE}_l = \frac{1}{K_l}\sum_{K=1}^{K_l} MSE_{l,k} \tag{13}$$

and K_l is the number of subbands for the *l*–th level decomposition. The optimum threshold, Eq. (10), applied to coefficients as soft thresholding and named weighted BayesShrink in transformed domain.

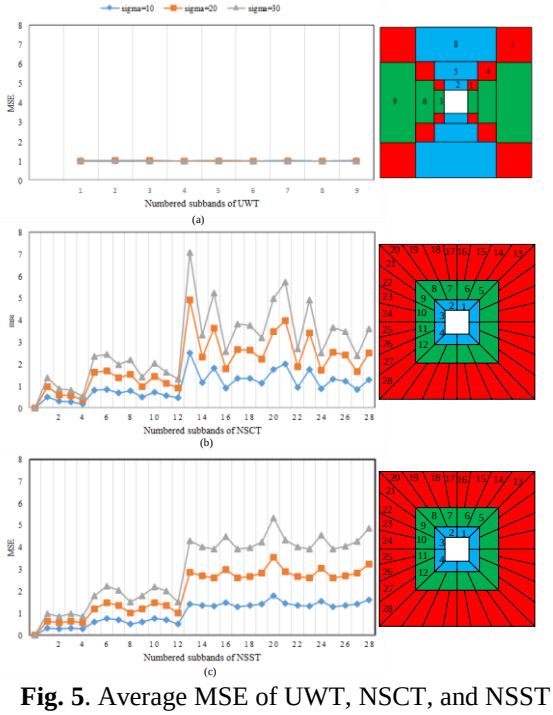

Fig. 5. Average MSE of UWT, NSCT, and NSST coefficients for ten independent trials, four different images, and three different noise variances. Shown the results for three levels decomposition of UWT (a), NSCT (b), and NSST (c)

As we use the weighted Bayesian shrinkage for three transformed domain, we named them WBS-UWT, WBS-NSCT, and WBS-NSST. Based on using these three transformation domains, we have performance comparison between Bayesian and weighted Bayesian.

4. EXPRIMENTAL RESULT

In order to compare how well the NSST is able to represent an image, we can plot the nonlinear approximation (NLA) curve. In this NLA experiment, we use Lena with size 512×512 pixels and 256 gray levels. The input image decomposed into three levels by UWT, NSCT, and NSST. We plot error as a function of the threshold level rather than the number of coefficient. Fig. 6 shows such curves for a threshold varying from 0 to 1. From top to bottom we see, UWT, NSCT, and NSST. From these curves, we conclude that, the UWT produces very poor result and the NSCT works much better than the UWT. The NSST yields the lowest approximation error among its competitors. Therefore, these experiments confirm that the NSST provide the best performance among the considered transforms.

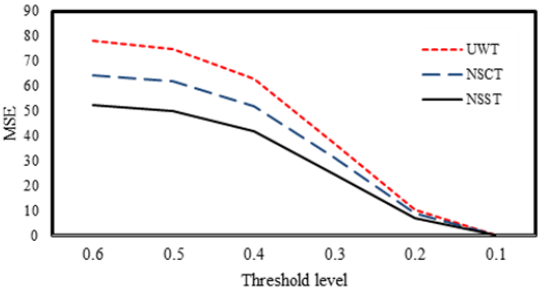

Fig. 6. Nonlinear approximation: Mean Square Error versus the threshold level for UWT, NSCT, and NSST.

In this section, we have compared the performance of BS with WBS in terms of subjective and objective image assessment when three introduced transforms, UWT, NSCT, and NSST, are used. The input noisy image is decomposed into three levels by UWT, NSCT, and NSST. Furthermore, all six algorithms run under the same circumstances. We used Barbara and Lena with size 512×512 pixels and 256 gray levels as the synthetic images and a real SAR image as well. Sample results of despeckled Barbara and a real SAR image shown in Figs. 7-8.

The performance evaluation of filters is a basic issue on SAR image despeckling. In this work, we used PSNR, SNR, MSE, noise variance (NV), mean square difference (MSD), and equivalent number of looks (ENL) as objective criteria parameters.

For any despeckled image, $\hat{S}$ the NV is

$$NV = \frac{\sum_{x=1}^{m}\sum_{y=1}^{n}[\hat{S}(x,y) - \overline{\hat{S}}(x,y)]^2}{mn} \quad (14)$$

Where $\overline{\hat{S}(x,y)} = \frac{1}{mn}\sum_{x=1}^{m}\sum_{y=1}^{n}\hat{S}(x,y)$ and mn refers to the image size. In general, NV determines the contents of speckle in an image. It means a lower variance gives a "smoother and cleaner" image as more speckle is removed though it does not necessarily depend on the intensity.

Fig. 7. Despeckling result of synthetic speckle image Barbara. (a) Original image, (b) speckled image with $\sigma = 30$, (c)-(h) despeckled images in order by BS-UWT,WBS-UWT, BS-NSCT, WBS-NSCT, BS-NSST and WBS-NSST.

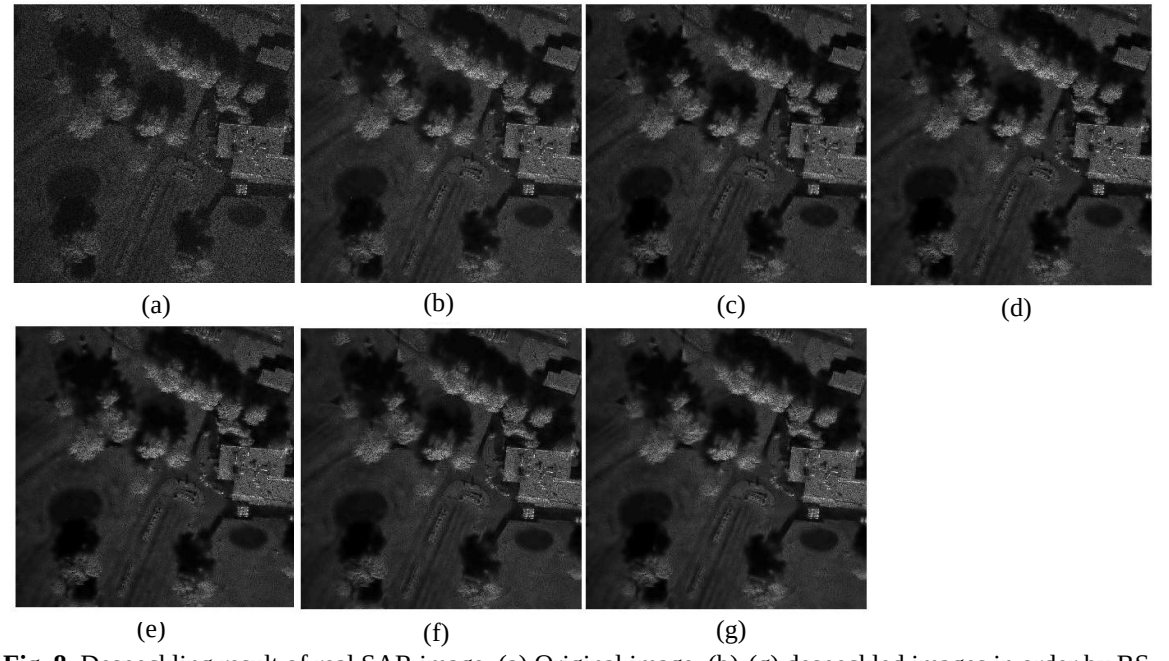

Fig. 8. Despeckling result of real SAR image. (a) Original image, (b)-(g) despeckled images in order by BS-UWT,WBS-UWT, BS-NSCT, WBS-NSCT, BS-NSST and WBS-NSST.

Another objective parameter, MSD, is

$$MSD = \frac{\sum_{x=1}^{m}\sum_{y=1}^{n}[\hat{S}(x,y) - S(x,y)]^2}{mn} \quad (15)$$

Where $\hat{S}$ refers to the despeckled image and S is the original image. Although, high MSD shows the significant filter performance, we should be careful about blurring edges.

ENL is known as the best objective assessment parameter,

$$ENL = \frac{\bar{\hat{S}}^2}{NV} \quad (16)$$

ENL estimates the speckle noise level in an image over uniform regions. In other words, getting great ENL value shows appropriate performance of an algorithm. As ENL value depends on the tested region size, we split an image into blocks with 16×16 pixels and compute ENL for each block separately and then write the average ENL. Unfortunately, ENL carries no information about the image resolution degradation, so, it is often used jointly with other parameters such as the Signal-to-Mean-Square-Error Ratio (S/MSE) or MSD.

The achieved results for Lena shown in Fig. 9, and for Barbara and the real SAR image are written in Tables I, II.

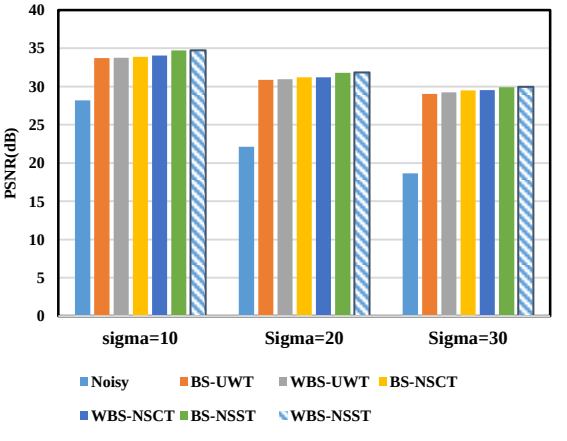

Fig. 9. Shown the obtained PSNR parameter to compare the performance of our method with five different approaches for Lena as the test image.

According to Figs. 7-9 and Tables I-II, we conclude:

- The proposed BS-NSST and WBS-NSST image denoising methods enjoy superior performance in terms of both subjective and objective evaluation over other denoising techniques especially they can remove noise and preserve edges and textures.
- The proposed BS-NSST, and WBS-NSST image denoising methods do not contain the quantity of disturbing artifacts along edges that one seen in other methods.
- The proposed weighted BayesShrink denoising methods WBS-UWT, WBS-NSCT, and WBS-NSST have better performance in term of subjective evaluation over BayesShrink denoising methods BS-UWT, BS-NSCT, and BS-NSST.
- When dealing with real SAR images, BS-NSST and WBS-NSST despeckling methods preserve most important point targets and texture structures.

5. CONCLUSION

In this paper, a new SAR image despeckling method is presented in undecimated wavelet, nonsubsampled Contourlet and nonsubsampled Shearlet transform domains based on the optimum threshold values. The optimum threshold values are obtained by BayesShrink where we consider noise efficiency factors for any subbands of each decomposition levels. In this way, WBS outperforms BS whenever the three UWT, NSCT, and NSST used as transformed domains. In addition, our experimental results based on objective and subjective criteria verify that WBS-NSST is the best method due to remove the most speckle noise and preserve the image edges and textures.

6. ACKNOWLEDGMENT

The authors would like to thank Sandia National Laboratories for providing the true SAR image used in this research. They are also grateful to DSP lab at Rice university for providing UWT algorithm [33].

Table 1. Obtained the objective assessment parameters in order to compare the performance of our proposed method with five different approaches where Barbara used as the test image.

	$\sigma = 10$			$\sigma = 20$			$\sigma = 30$		
	MSE	PSNR(dB)	SNR	MSE	PSNR(dB)	SNR	MSE	PSNR(dB)	SNR
Noisy Image	99.88	28.17	13.48	400.47	22.13	7.45	896.78	18.63	5.21
BS-UWT	37.50	31.45	17.77	98.18	28.21	13.52	181.42	25.58	11.48
WBS-UWT	37.50	31.45	17.77	98.93	28.21	13.52	181.28	25.58	11.48

BS-NSCT	33.22	32.82	18.13	72.22	29.57	14.89	114.50	27.50	12.88
WBS-NSCT	33.89	32.86	18.17	71.27	29.63	14.94	114.46	27.57	12.89
BS-NSST	26.54	33.92	19.23	61.32	30.28	15.60	108.55	27.80	13.12
WBS-NSST	**26.50**	**33.93**	**19.24**	**61.25**	**30.29**	**15.60**	**108.53**	**27.80**	**13.12**

Table 2. Obtained the objective assessment parameters for different methods where we used the real SAR image.

	NV	*MSD*	*ENL*
Noisy Image	1.104	0	8.980980
BS-UWT	0.36	0.0017	50.38
WBS-UWT	0.31	0.0021	64.07
BS-NSCT	0.29	0.0020	89.45
WBS-NSCT	0.27	0.0021	100.54
BS-NSST	0.26	0.0023	125.57
WBS-NSST	**0.24**	**0.0025**	**145.73**

REFERENCES

[1] J.-S. Lee, L. Jurkevich, P. Dewaele, P. Wambacq, and A. Oosterlinck, **"Speckle filtering of synthetic aperture radar images: A review,"** *Remote Sensing Reviews*, Vol. 8, pp. 313-340, 1994.

[2] V. S. Frost, J. A. Stiles, K. S. Shanmugan, and J. C. Holtzman, **"A model for radar images and its application to adaptive digital filtering of multiplicative noise,"** *IEEE Transactions on Pattern Analysis and Machine Intelligence*, Vol. 4, pp. 157-66, Feb 1982.

[3] D. Kuan, A. Sawchuk, T. Strand, and P. Chavel, **"Adaptive restoration of images with speckle,"** *IEEE Transactions on Acoustics, Speech and Signal Processing*, Vol. 35, pp. 373-383, 1987.

[4] L. I. Rudin, S. Osher, and E. Fatemi, **"Nonlinear total variation based noise removal algorithms,"** *Physica D: Nonlinear Phenomena*, Vol. 60, pp. 259-268, 1992.

[5] S. G. Chang, B. Yu, and M. Vetterli, **"Adaptive wavelet thresholding for image denoising and compression,"** *IEEE Transactions on Image Processing*, Vol. 9, pp. 1532-1546, 2000.

[6] L. Sendur and I. W. Selesnick, **"Bivariate shrinkage functions for wavelet-based denoising exploiting interscale dependency,"** *IEEE Transactions on Signal Processing*, Vol. 50, pp. 2744-2756, 2002.

[7] D. Gleich and M. Datcu, **"Wavelet-based despeckling of SAR images using Gauss–Markov random fields,"** *IEEE Transactions on Geoscience and Remote Sensing*, Vol. 45, pp. 4127-4143, 2007.

[8] G. Chen and X. Liu, **"Contourlet-based despeckling for SAR image using hidden Markov tree and Gaussian Markov models,"** *in 1st Asian and Pacific Conference on Synthetic Aperture Radar*, 2007, pp. 784-787.

[9] B. Hou, X. Zhang, X. Bu, and H. Feng, **"SAR image despeckling based on nonsubsampled shearlet transform,"** *IEEE Journal of Selected Topics in Applied Earth Observations and Remote Sensing*, Vol. 5, pp. 809-823, 2012.

[10] E. J. Candes and D. L. Donoho, **"Curvelets: A surprisingly effective nonadaptive representation for objects with edges,"** *Stanford University Department of Statistics* 2000.

[11] M. N. Do and M. Vetterli, **"Contourlets: a directional multiresolution image representation,"** *in International Conference on Image Processing*, 2002, pp. I-357-I-360.

[12] D. Labate, W.-Q. Lim, G. Kutyniok, and G. Weiss, **"Sparse multidimensional representation using shearlets,"** *in Optics & Photonics 2005*, pp. 59140U-59140U.

[13] N. Kingsbury, **"Image processing with complex wavelets,"** *Philosophical Transactions of the Royal Society of London. Series A: Mathematical, Physical and Engineering Sciences*, Vol. 357, pp. 2543-2560, 1999.

[14] E. J. Candès and D. L. Donoho, **"Ridgelets: A key to higher-dimensional intermittency,"** *Philosophical Transactions of the Royal Society of London. Series A: Mathematical, Physical and Engineering Sciences*, Vol. 357, pp. 2495-2509, 1999.

[15] M. Holschneider, R. Kronland-Martinet, J. Morlet, and P. Tchamitchian, **"A real-time algorithm for signal analysis with the help of the wavelet transform,"** *ed: Springer*, 1990, pp. 286-297.

[16] S. Mallat, **"Zero-crossings of a wavelet transform,"** *IEEE Transactions on Information Theory*, Vol. 37, pp. 1019-1033, 1991.

[17] A. L. Da Cunha, J. Zhou, and M. N. Do, **"The nonsubsampled contourlet transform: theory, design, and applications,"** *IEEE Transactions on Image Processing*, Vol. 15, pp. 3089-3101, 2006.

[18] G. Easley, D. Labate, and W.-Q. Lim, **"Sparse directional image representations using the discrete shearlet transform,"** *Applied and Computational Harmonic Analysis*, Vol. 25, pp. 25-46, 2008.

[19] H. Guo, **"Theory and applications of the shift-invariant, time-varying and undecimated wavelet transforms,"** *PhD dissertation, Rice University*, 1995.

[20] C. Oliver and S. Quegan, **Understanding Synthetic Aperture Radar Images with CDROM: SciTech Publishing**, 2004.

[21] J. W. Goodman, **"Some fundamental properties of speckle,"** *JOSA*, Vol. 66, pp. 1145-1150, 1976.

[22] M. Kociołek, A. Materka, M. Strzelecki, and P. Szczypiński, **"Discrete wavelet transform-derived features for digital image texture analysis,"** in *International Conference on Signals and Electronic Systems*, Łódź-Poland, 2001, pp. 99-104.

[23] K. Sankar and K. Nirmala, **"Nonsubsampled Contourlet Transformation Based Image Enhancement with Spatial and Statistical Feature Extraction for Classification of Digital Mammogram,"** *International Journal of Soft*

Computing and Engineering, Vol. 3, pp. 108-110, 2013.

[24] S. Dahlke, G. Steidl, and G. Teschke, **"Shearlet coorbit spaces: compactly supported analyzing shearlets, traces and embeddings,"** *Journal of Fourier Analysis and Applications*, Vol. 17, pp. 1232-1255, 2011.

[25] D. L. Donoho and I. M. Johnstone, **"Threshold selection for wavelet shrinkage of noisy data,"** in *Engineering in Medicine and Biology Society*, 1994. Engineering Advances: New Opportunities for Biomedical Engineers. Proceedings of the 16th Annual International Conference of the IEEE, 1994, pp. A24-A25.

[26] D. L. Donoho and I. M. Johnstone, **"Adapting to unknown smoothness via wavelet shrinkage,"** *Journal of the American Statistical Association*, Vol. 90, pp. 1200-1224, 1995.

[27] D. L. Donoho and J. M. Johnstone, **"Ideal spatial adaptation by wavelet shrinkage,"** *Biometrika*, Vol. 81, pp. 425-455, 1994.

[28] R. K. Rai, J. Asnani, and T. Sontakke, **"Review of Shrinkage Techniques for Image Denoising,"** *International Journal of Computer Applications*, Vol. 42, pp. 13-16, 2012.

[29] D.-X. Zhang, Q.-W. Gao, and X.-P. Wu, **"Bayesian-based speckle suppression for SAR image using contourlet transform,"** *Journal of Electronic Science and Technology of China*, Vol. 6, pp. 79-82, 2008.

[30] H. A. Chipman, E. D. Kolaczyk, and R. E. McCulloch, **"Adaptive Bayesian wavelet shrinkage,"** *Journal of the American Statistical Association*, Vol. 92, pp. 1413-1421, 1997.

[31] L. Sendur and I. W. Selesnick, **"Bivariate shrinkage with local variance estimation,"** *IEEE Signal Processing Letters*, Vol. 9, pp. 438-441, 2002.

[32] M. Kiani and S. Ghofrani, **"Two new methods based on Contourlet transform for despeckling SAR images,"** *Journal of Applied Remote Sensing Manuscript submitted for publication.*, 2014.

[33] Rice lab homepage: http://www.dsp.rice.edu.